Supplementary Material for
Gate-tunable negative differential conductance in hybrid semiconductor-superconductor devices

Ming-Li Liu(刘明黎)[1,2†], Dong Pan(潘东)[3†], Tian Le(乐天)[1], Jiang-Bo He(贺江波)[1], Zhong-Mou Jia(贾仲谋)[1,2], Shang Zhu(朱尚)[1,2], Guang Yang(杨光)[1], Zhao-Zheng Lyu(吕昭征)[1], Guang-Tong Liu(刘广同)[1,4], Jie Shen(沈洁)[1,4], Jian-Hua Zhao(赵建华)[3**], Li Lu(吕力)[1, 2, 4**], and Fan-Ming Qu(屈凡明)[1,2,4**]

[1] *Beijing National Laboratory for Condensed Matter Physics, Institute of Physics, Chinese Academy of Sciences, Beijing 100190, China*
[2] *School of Physical Sciences, University of Chinese Academy of Sciences, Beijing 100049, China*
[3] *State Key Laboratory of Superlattices and Microstructures, Institute of Semiconductors, Chinese Academy of Sciences, P.O. Box 912, Beijing 100083, China*
[4] *Songshan Lake Materials Laboratory, Dongguan 523808, China*

[†]These authors contributed equally to this work.
[**]Corresponding author. Email: jhzhao@semi.ac.cn; lilu@iphy.ac.cn; fanmingqu@iphy.ac.cn

1. Scanning electron microscope (SEM) image of Device A

For both types of devices, the superconducting electrodes (S) are fabricated using standard electron-beam lithography followed by electron-beam evaporation of Al (~80 nm). The normal electrodes (N) are fabricated by selectively etching away the Al layer prior to a direct deposition of Ti/Au (8 nm/80 nm) using a double-layer resist. Short junctions less than 50 nm between N and the superconducting nanowire (SNW) can be realized by utilizing the undercut structure of the double-layer resist and such one-step fabrication process.

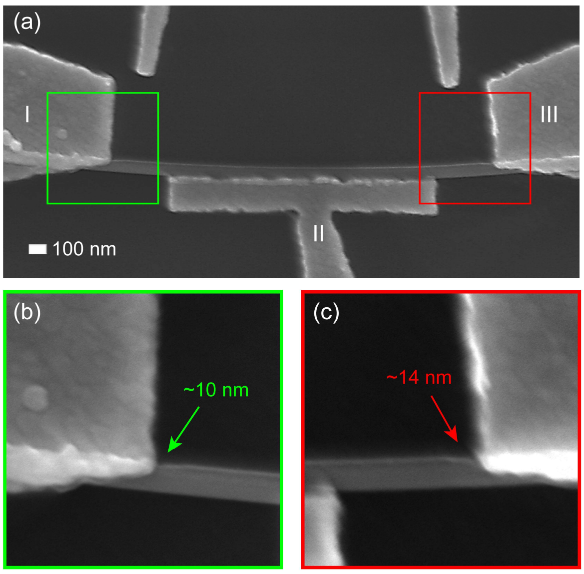

Fig. S1. (a) SEM image of Device A. The corresponding schematic diagram is shown in Fig. 1(a) in the main text. (b, c) Zoom-in of the green and red box area in (a), respectively. The left junction segment is ~10 nm, and the right is ~14 nm.

2. Additional data on device A

This section shows additional data on device A.

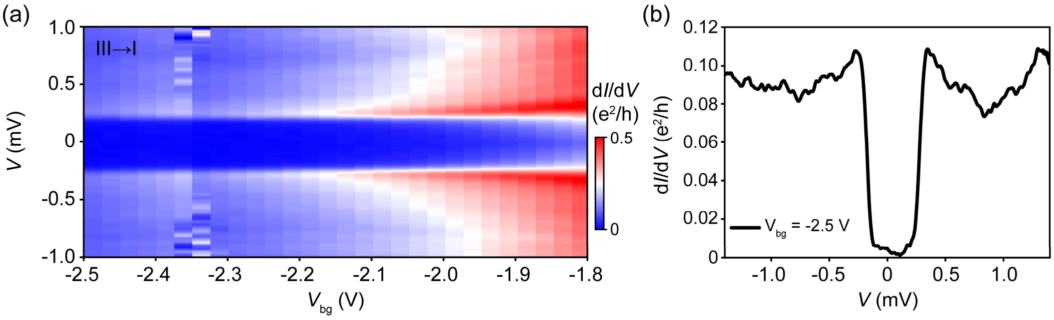

Fig. S2. Additional data on Device A for electrodes III→I at larger barrier strength. (a) The differential conductance $\mathrm{d}I/\mathrm{d}V$ as a function of bias voltage V and back-gate voltage V_{bg} for electrodes III→I. (b) The differential conductance $\mathrm{d}I/\mathrm{d}V$ linecut at $V_{\mathrm{bg}} = -2.5$ V. A hard gap[1] can be inferred from the ratio between the normal and superconducting state conductance, $G_N/G_S{\sim}90$.

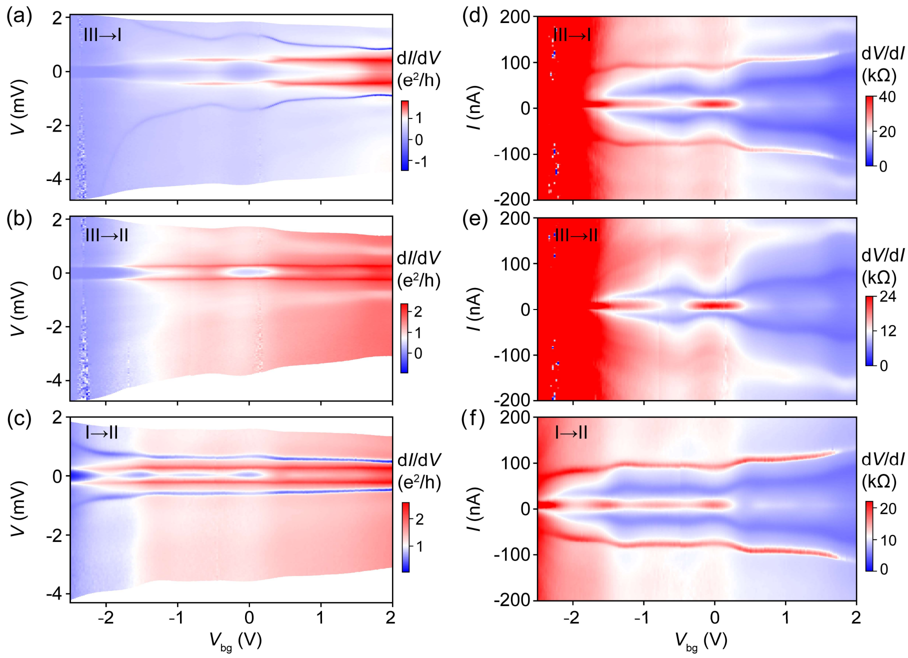

Fig. S3. (a-c) The measured $\mathrm{d}I/\mathrm{d}V$ spectroscopy in the voltage-driven mode (sweeping voltage) for electrodes III→I, III→II and I→II, respectively. (d-f) The measured $\mathrm{d}V/\mathrm{d}I$ spectroscopy in the current-driven mode (sweeping current) for electrodes III→I, III→II and I→II, respectively. (a, b, d) The same as Fig. 1(b), Fig. 1(d), and Fig. 2(a), respectively. For clarity and a direct comparison, we plot these three figures here again.

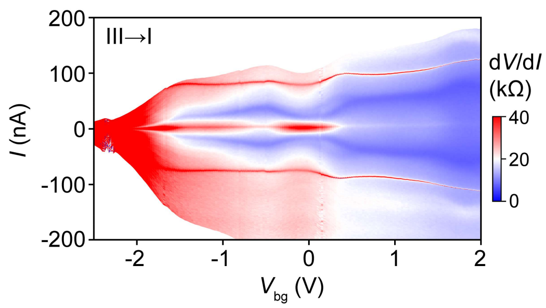

Fig. S4. The result of transforming $\mathrm{d}I/\mathrm{d}V$ [Fig. 1(b) in main text, i.e., Fig. S3(a)] to $\mathrm{d}V/\mathrm{d}I$. I is calculated by $\int (dI/dV)\, dV$. The transformed $\mathrm{d}V/\mathrm{d}I$ peaks from the voltage-driven measurement show the same behavior as the current-driven measurement, i.e., Fig. S3(d).

3. Additional data on device B

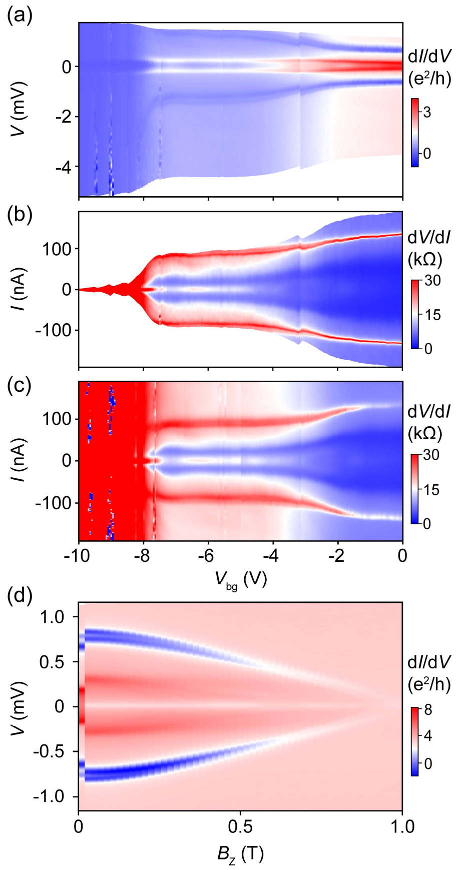

Fig. S5. (a) The measured $\mathrm{d}I/\mathrm{d}V$ spectroscopy in the voltage-driven mode for device B. The differential conductance dip disappears at $V_{\mathrm{bg}} \approx -8$ V. (b) The result of transforming $\mathrm{d}I/\mathrm{d}V$ in (a) to $\mathrm{d}V/\mathrm{d}I$. (c) The measured $\mathrm{d}V/\mathrm{d}I$ spectroscopy in the current-driven mode. (d) 2D $\mathrm{d}I/\mathrm{d}V$ map showing the evolution of the dip in magnetic field at $V_{\mathrm{bg}} = -2$ V. The conductance jump near zero magnetic field is caused by the quench of evaporated Al.

4. Details of the theoretical simulation

As explained in the main text, the transport of our semiconductor-superconductor hybrid devices is described by the BTK-supercurrent model. According to the BTK theory[2], the normal metal-superconductor (NS) interface potential barrier is assumed to be a one-dimensional delta function $V_{NS} = V_0\delta(x)$. When a voltage is applied, the current could be calculated as

$$I = 2N(0)ev_F S\int_{-\infty}^{+\infty}[f_0(E-eV) - f_0(E)]\,[1 + A(E) - B(E)]dE,$$

where $N(0)$ is the density of states at the Fermi level, S is the effective area of the NS interface, f_0 is Fermi-Dirac distribution function, $f_0(E-eV) = [1+\exp\left(\frac{E-eV}{k_B T}\right)]^{-1}$, k_B is Boltzmann constant, T is temperature. $A(E)$ is the probability of Andreev reflection, $A = {u_0^2 v_0^2}/{\gamma^2}$, and $B(E)$ is the probability of normal electron reflection, $B = {(u_0^2 - v_0^2)^2 Z^2(1+Z^2)}/{\gamma^2}$, where $u_0^2 = 1 - v_0^2 = \frac{1}{2}(1 + [(E^2 - \Delta^2/E^2)]^{1/2})$, $\gamma^2 = [u_0^2 + Z^2(u_0^2 - v_0^2)]^2$, and $Z = V_0/\hbar v_F$ is a dimensionless parameter that represents the barrier strength. When $Z = 0$, the barrier is transparent and $A = 1$. The differential conductance of the NS interface can be written as

$$\frac{dI}{dV} = 2N(0)ev_F S \int_{-\infty}^{+\infty} \frac{\partial f_0(E-e\ )}{\partial (eV)} [1 + A(E) - B(E)]dE.$$

Considering the inelastic scattering of the interface, the Bogoliubov coherence factors u_0 and v_0 need to be rewritten as

$$u_0^2 = \frac{1}{2}\left[1 + \frac{\sqrt{(E+i\Gamma)^2-\Delta^2}}{E+i\Gamma}\right] = 1 - v_0^2,$$

where Γ is the strength of inelastic scattering, $\Gamma = \hbar/\tau$, τ is the lifetime of the quasiparticles. When $\Gamma = 0$, no inelastic scattering occurs at the NS interface. However, with the increase of Γ, the broadening of the Andreev peak increases and the intensity decreases. The experimental data in the superconducting energy gap can be simulated well by using parameters: Γ, Δ, T, Z, R_{BTK}^N. The resistance R_{BTK}^N is the R_{BTK} at high-bias voltage used to match the real resistance in the data.

However, the NDCs and the differential conductance dips cannot be simulated by BTK model. Therefore, we add the external supercurrent part on the basis of BTK model, mainly considering the critical supercurrent effect of SNW (superconducting nanowire), and we call it the BTK-supercurrent model. Assuming that R_{SC} is the resistance of the SNW, when the SNW is superconducting, $R_{SC} = 0$; when the current I is greater than the critical supercurrent I_c, $R_{SC} = R_{SC}^N$ (the normal-state resistance of the SNW). The $I - V$ function of the SNW part can be written as $V_{SC} = R_{SC}^N\sqrt{I^2 - I_c^2}$ [3]. Considering the finite temperature and disorder, $I + i\gamma_c$ is used to replace I to adjust the broadening near the critical supercurrent, and thus $V_{SC} = R_{SC}^N\sqrt{(I + i\gamma_c)^2 - I_c^2}$. The total resistance can be written as: $R_{tol} = R_{BTK} + R_{SC}$. Taking the parameters of the superconductor part, i.e., I_c, R_{SC}^N, γ_c, into account, and combining with the BTK parameters, Γ, Δ, T, Z, R_{BTK}^N, we can simulate our experimental results.

For Fig. 4(g) in the main text, some parameters are rewritten as a function of V_{bg} to simulate the variation trend with V_{bg}. Since we cannot determine the exact relations between these parameters and V_{bg}, we just assume function forms phenomenologically, as shown in Table 1.

Part: R_{BTK}		**Part: R_{SC}**	
Γ (meV)	0.03	I_c (nA)	$0.3 * \exp(V_{\mathrm{bg}}) + 0.4$
Δ (meV)	0.46		
T (K)	0.03	$R_{\mathrm{SC}}^{\mathrm{N}}$ (h/e^2)	0.2
Z	$2/(V_{\mathrm{bg}} + 4)$	γ_c (nA)	$0.008 * \exp(1 - V_{\mathrm{bg}})$
$R_{\mathrm{BTK}}^{\mathrm{N}}$ (h/e^2)	$1/\exp(V_{\mathrm{bg}} - 1)$		

Table 1: Parameters used for Fig. 4(g) in the main text.

Using our BTK-supercurrent model, the three curves in Fig. 1(c) in the main text can be simulated well, as shown in Fig. S6 (see Table 2 for corresponding parameters).

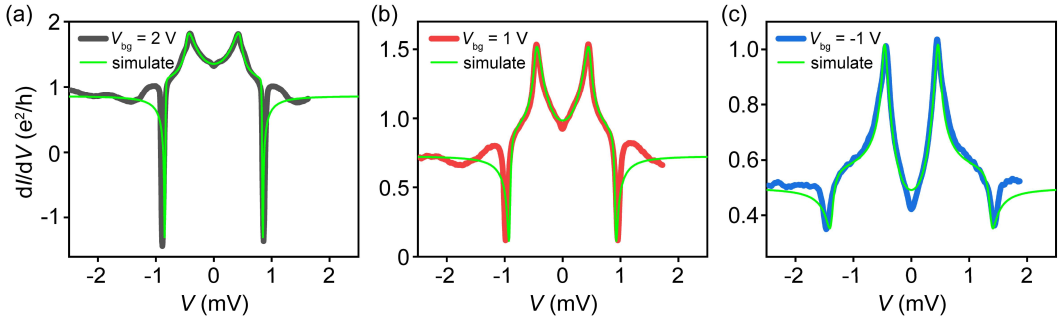

Fig. S6. Simulation of the experiment data shown in Fig. 1(c) in the main text. The measured $\mathrm{d}I/\mathrm{d}V$ vs. V curves at $V_{\mathrm{bg}} = 2$ V, 1 V, -1 V correspond to the black, red, blue linecuts, respectively. The green lines are the simulation results using our BTK-supercurrent model.

	Part: R_{BTK}					**Part: R_{SC}**		
Parameters	Γ **(meV)**	Δ **(meV)**	T **(K)**	Z	$R_{\mathrm{BTK}}^{\mathrm{N}}$ (h/e^2)	I_c **(nA)**	$R_{\mathrm{SC}}^{\mathrm{N}}$ (h/e^2)	γ_c **(nA)**
$V_{\mathrm{bg}} = 2$ **V**	0.03	0.46	0.03	0.4	0.96	120	0.2	0.002
$V_{\mathrm{bg}} = 1$ **V**	0.03	0.47	0.03	0.48	1.16	103	0.2	0.018
$V_{\mathrm{bg}} = -1$ **V**	0.03	0.475	0.03	0.64	1.78	90	0.2	0.03

Table 2: Parameters used for Figs. S6(a-c).

5. The effect on the NDC of the ratio between $R_{\mathrm{BTK}}^{\mathrm{N}}$ and $R_{\mathrm{SC}}^{\mathrm{N}}$

As we mentioned in the main text, the depth of the NDC decreases with the increase of $R_{\mathrm{BTK}}^{\mathrm{N}}$, and increases with the increase of $R_{\mathrm{SC}}^{\mathrm{N}}$. Here, we discuss how the ratio between $R_{\mathrm{BTK}}^{\mathrm{N}}$ and $R_{\mathrm{SC}}^{\mathrm{N}}$ affects the evolution of the NDC. As shown in Fig. S7(a), for a fixed $R_{\mathrm{BTK}}^{\mathrm{N}}/R_{\mathrm{SC}}^{\mathrm{N}} = 2$, however, when $R_{\mathrm{BTK}}^{\mathrm{N}}$ and $R_{\mathrm{SC}}^{\mathrm{N}}$ increase proportionally, the depth of the NDC presents a very big difference. For $R_{\mathrm{BTK}}^{\mathrm{N}}/R_{\mathrm{SC}}^{\mathrm{N}} = 4$, as shown in Fig. S7(b), a similar behavior is present. If we compare the curves with the same color, i.e., the same $R_{\mathrm{BTK}}^{\mathrm{N}}$, the depth of the NDC is less in Fig. S7(b) than that in Fig. S7(a). Therefore, the NDC is not only determined by the ratio between $R_{\mathrm{BTK}}^{\mathrm{N}}$ and $R_{\mathrm{SC}}^{\mathrm{N}}$, but the size of $R_{\mathrm{BTK}}^{\mathrm{N}}$ and $R_{\mathrm{SC}}^{\mathrm{N}}$ also plays a role.

Note that $R_{\mathrm{BTK}}^{\mathrm{N}}$ not only affects the depth of the NDC, but also changes the corresponding bias position of the NDC, as shown in Fig. S7(c). When $R_{\mathrm{SC}}^{\mathrm{N}}$ is fixed at 0.5 h/e^2, with the increase of the ratio between $R_{\mathrm{BTK}}^{\mathrm{N}}$ and $R_{\mathrm{SC}}^{\mathrm{N}}$, the depth of the NDC decreases, and the NDC moves to higher $|V|$ simultaneously. When $R_{\mathrm{BTK}}^{\mathrm{N}}$ is fixed, with the increase of the ratio, the depth of the NDC increases, and the position of the NDC does not change, as shown in Fig. S7(d). In a word, the evolution of the NDC is a function of $R_{\mathrm{BTK}}^{\mathrm{N}}$ and $R_{\mathrm{SC}}^{\mathrm{N}}$, not only of the ratio.

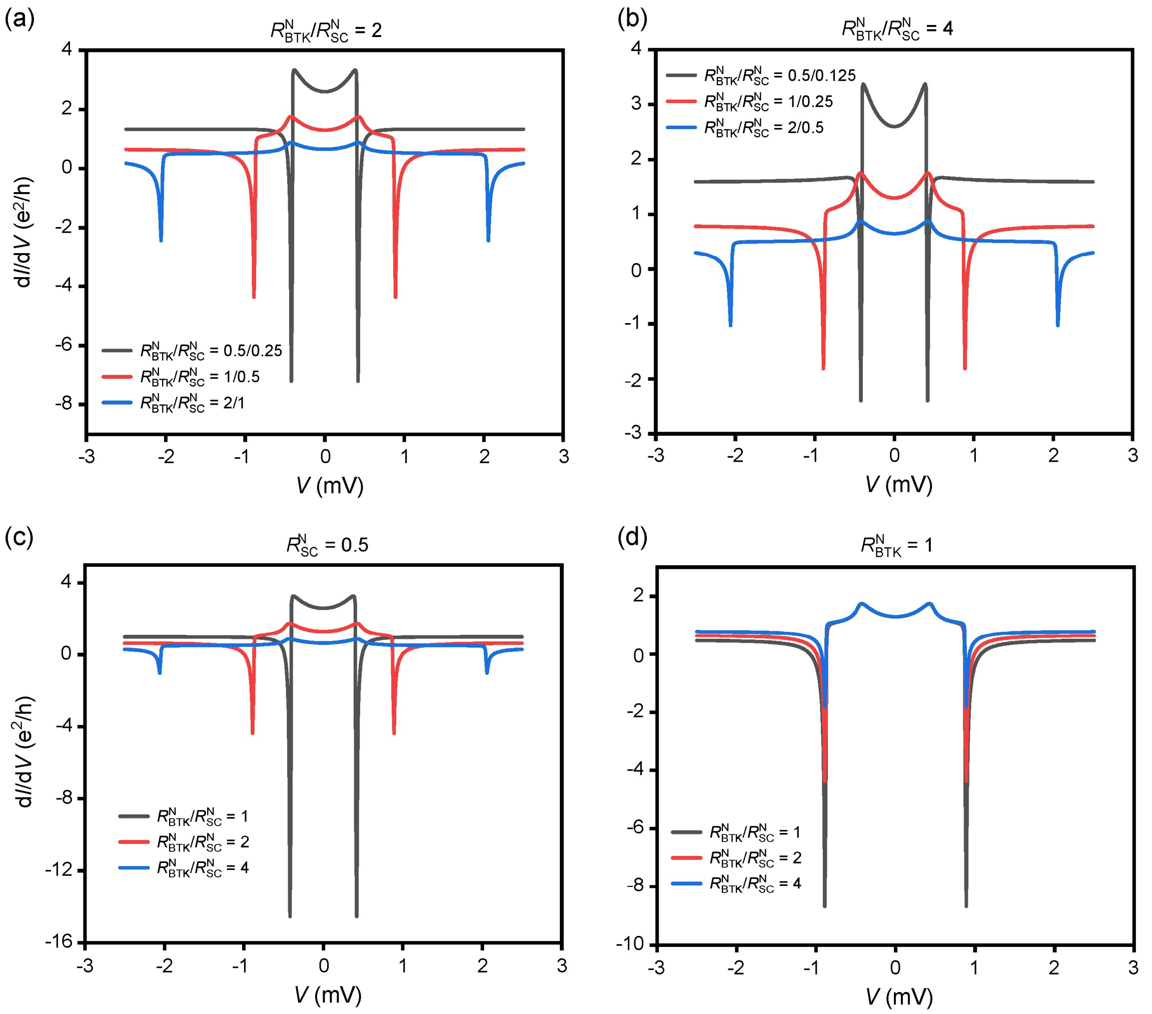

Fig. S7. (a, b) Simulation results for a ratio between $R^{\mathrm{N}}_{\mathrm{BTK}}$ and $R^{\mathrm{N}}_{\mathrm{SC}}$ of 2 and 4, respectively. Black, red and blue lines correspond to different $R^{\mathrm{N}}_{\mathrm{BTK}}$ and $R^{\mathrm{N}}_{\mathrm{SC}}$ (in unit of h/e^2). (c, d) Simulation results for fixed $R^{\mathrm{N}}_{\mathrm{BTK}}$ and $R^{\mathrm{N}}_{\mathrm{SC}}$, respectively. The rest simulation parameters of the four figures are: $\Gamma = 0.03$ meV, $\Delta = 0.46$ meV, $T = 0.03$ K, $Z = 0.4$, $I_c = 120$ nA, $\gamma_c = 0.002$ nA.

Supplemental references

[1] Chang W, Albrecht S M, Jespersen T S, Kuemmeth F, Krogstrup P, Nygard J and Marcus C M 2015 *Nat. Nanotechnol.* **10** 232

[2] Blonder G E, Tinkham M and Klapwijk T M 1982 *Phys. Rev. B* **25** 4515

[3] Kumar R and Sheet G 2021 *Phys. Rev. B* **104** 094525